of such a chelate, that is, the direct correlation of the crystalline and solution circular dichroism spectra with crystallographic results, rather than the more empirical assignments based on the use of model ligands, more kinetically inert metal-ion complexes, or closely related compounds relied on much in the past. Two additional conclusions can be drawn from our observations. In the case of ferric chelates of biological interest, it is necessary to compare the absolute configuration of the molecule in the solid state with that in solution. This communication represents such an example, and, in absence of an anomalous dispersion experiment, single-crystal and solution circular dichroism spectroscopy offers a seemingly satisfactory method. Our results can also be used to rationalize the apparent inactivity of the *Penicillium* esterase toward the aluminum chelate of *N,N',N"*-triacetyl-fusarinine[14] by assuming stereochemical specificity of the esterase and a slow rate of equilibrium for the chelate. Finally, it is noteworthy that our findings do not allow the prediction of which diasteroisomer (Λ-cis or Δ-cis) of ferric *N,N',N"*-triacetylfusarinine is actively transported across the microbial cell membrane. Experimentally, this question will be approached by performing the transport experiments with chromatographically resolved diastereoisomers of the chelate of a kinetically inert metal ion, such

as Cr(III) or Co(III). This method was successfully used in probing the transport of ferrichrome in *Ustilago sphaerogena*, using resolved Λ-cis and Δ-cis chromic deferriferrichrome.[42]

Supplementary Material Available: A listing of structure amplitudes, anisotropic thermal parameters of nonhydrogen atoms, and hydrogen atom parameters (33 pages). Ordering information is given on any current masthead page.

(42) Leong, J.; Neilands, J. B.; Raymond, K. N. *Biochem. Biophys. Res. Commun.* **1974**, *60*, 1066-1071.

Synthesis and Crystal and Molecular Structure of [(Ph₃P)₂N⁺][S₄N⁻] and the Electronic Structure of the Planar Acyclic Anion, S₄N⁻[1]

T. Chivers,* W. G. Laidlaw, R. T. Oakley, and M. Trsic

Contribution from the Department of Chemistry, University of Calgary, Calgary T2N 1N4, Alberta, Canada. Received February 5, 1980

Abstract: The thermal decomposition of PPN⁺S₄N₅⁻ [PPN⁺ = (Ph₃P)₂N⁺] in acetonitrile at 78 °C leads, sequentially, to the corresponding salts of the S₃N₃⁻ and S₄N⁻ anions. The crystal and molecular structure of the dark blue salt, PPN⁺S₄N⁻, has been determined by X-ray crystallography. The compound crystallized in the space group P1̄, triclinic, a = 11.220 (2) Å, b = 16.860 (3) Å, c = 9.862 (2) Å, α = 99.17 (1)°, β = 98.04 (1)°, γ = 71.56 (1)°, V = 1739.2 Å³, and Z = 2. The refined structure (R_1 = 0.064) shows that the S₄N⁻ anion is an essentially planar, cis,trans chain with nitrogen as the central atom. The terminal S–S bond distances are remarkably short (1.879 (3) and 1.943 (2) Å), while the S–N bond lengths show a pronounced inequality (1.667 (5) and 1.521 (5) Å). The bond angles at the internal sulfur atoms are ca. 110.5 (2)° and the angle at nitrogen is 120.8 (3)°. Infrared and Raman spectra of PPN⁺S₄N⁻ and PPN⁺S₄*N⁻ (where *N = 30% ¹⁵N) demonstrate that the vibrational frequencies at ca. 592 and 565 cm⁻¹ can be assigned to the stretching modes of the unequal S–S bonds. Ab initio Hartree–Fock–Slater SCF calculations have been carried out for S₄N⁻ and show that the calculated statistical energy of the experimental conformation is not substantially lower than that of the symmetrical cis,trans or trans,trans conformations of the anion. The ground-state electronic structure of S₄N⁻ is an 8π-electron system. The strong absorption in the visible spectrum at 582 nm appears to be the result of a π*(HOMO)→π*(LUMO) transition. The S–N linkages can be described approximately as net ²/₃σ plus ¹/₂π bonds, while the S–S bonds are approximately ⁵/₄σ plus ¹/₄π. The terminal sulfur atoms each carry two lone pairs of electrons and bear large negative charges, −0.42 and −0.44, as does the nitrogen, −0.35; the internal sulfur atoms have one lone pair of electrons and have small positive charges, +0.01 and +0.20. The experimental conformation may be the result of an electrostatic interaction between terminal and internal sulfur atoms.

Introduction

The formation of a blue color on deprotonation of cyclic sulfur imides, e.g., S₇NH, in basic media is used as a spot test in the chromatographic separation of these imides for *cyclo*-S₈.[2] The same deep blue color is also dramatically apparent during the preparation of sulfur imides from (a) sulfur monochloride and ammonia in DMF[2] or (b) sodium azide and *cyclo*-S₈ in HMPA.[3] A number of attempts to identify the species responsible for the

blue color have been made. The suggestion that it is a neutral sulfur radical Sₓ (x = 2–4)[4] was shown to be incorrect by Chapman and Massey, who demonstrated that it was negatively charged and diamagnetic; they proposed it to be the S₇N⁻ anion.[5] Subsequent work by Olsen and Olsen established the presence of *cyclo*-S₇N⁻ in solutions resulting from the deprotonation of S₇NH with various bases.[6] On the basis of detailed studies of the alkylation of such solutions, these workers suggested that *cyclo*-S₇N⁻ was in equilibrium with other anions, including an "open-

(1) For a preliminary communication see: Chivers, T.; Oakley, R. T. *J. Chem. Soc., Chem. Commun.* **1979**, 752.
(2) Heal, H. G.; Kane, J. *Inorg. Synth.* **1968**, *11*, 184.
(3) (a) Bojes, J.; Chivers, T. *J. Chem. Soc., Dalton Trans.* **1975**, 1715. (b) Bojes, J.; Chivers, T.; Drummond, I. *Inorg. Synth.* **1978**, *18*, 203.

(4) Lux, H.; Anslinger, H. *Chem. Ber.* **1961**, *94*, 1161.
(5) Chapman, D.; Massey, A. G. *Trans. Faraday Soc.* **1962**, *58*, 1291.
(6) (a) Olsen, B. A.; Olsen, F. P. *Inorg. Chem.* **1969**, *8*, 1736. (b) Tingle, E. M.; Olsen, F. P. *Ibid.* **1969**, *8*, 1741.

chain" anion.[6] In 1973, Mendelsohn and Jolly reported the preparation of cyclo-S_7N^- from S_7NH and powdered KOH in THF.[7] These workers showed that the cyclic anion was yellow and stable at -78 °C but that, on warming above -40 °C, it spontaneously isomerized, probably to an open-chain form of S_7N^-; they were unable to decide if the latter species was responsible for the predominantly blue color of $K^+S_7N^-$ solutions at 0 °C.[7] In the same year, Chivers and Drummond described the isolation and characterization of a dark blue salt, n-$Bu_4N^+S_4N^-$, following the deprotonation of cyclo-S_7NH with tetra-n-butylammonium hydroxide in diethyl either.[8] This product was obtained, mixed with cyclo-S_8, by the disproportionation of yellow n-Bu_4N^+-cyclo-S_7N^- at 23 °C. On the basis of a comparison of the vibrational spectra with those of the isoelectronic CS_4^{2-} ion,[9] a branched-chain structure was proposed for S_4N^-.[8b] Such a structure has now been confirmed for CS_4^{2-} by X-ray crystallography.[10] However, numerous attempts in our laboratory to obtain crystals of S_4N^-, with different cations, have been unsuccessful until the present study.

As part of our investigations of the thermolysis of S–N compounds we have discovered that the $S_4N_5^-$ ion decomposes smoothly in boiling acetonitrile to give the S_4N^- anion and, as a salt with PPN^+, crystals suitable for X-ray crystallography can be obtained.[1] In this paper we report the full details of the synthesis and crystal and molecular structure of $PPN^+S_4N^-$. In addition we have carried out ab initio Hartree–Fock–Slater (HFS) SCF calculations of S_4N^- in order to (a) obtain an MO description of the ground-state electronic structure, (b) determine the energy of the experimental conformation relative to other conformations, (c) ascertain the importance, if any, of long-range S–S interactions in the anion, and (d) assign the intense absorption in the visible spectrum to the appropriate electronic transition.

Experimental Section

Materials. Tetrasulfur tetranitride was prepared according to the literature method.[11]   Piperidinium tetrasulfur pentanitride, $(CH_2)_5NH_2^+S_4N_5^-$, was prepared by the reaction of anhydrous piperidine with S_4N_4 in absolute ethanol.[12] Bis(triphenylphosphine)iminium tetrasulfur pentanitride, $PPN^+S_4N_5^-$, was then prepared by cation exchange of $(CH_2)_5NH_2^+S_4N_5^-$ with PPN^+Cl^- (Aldrich) in water (yield ca. 100%). The crude, yellow precipitate was recrystallized from hot acetonitrile to give air-stable, yellow needles of $PPN^+S_4N_5^-$, which showed infrared bands characteristic of the $S_4N_5^-$ anion at 955 s, 916 s, 757 m, 747 m, 666 w, 647 w, 598 m, 428 m, and 300 vw cm^{-1}.[12,13] The UV–visible spectrum (in CH_2Cl_2) had a band at 293 nm, $\epsilon \sim 5.9 \times 10^3$ L mol^{-1} cm^{-1}, with a shoulder at 345 nm, $\epsilon \sim 2.5 \times 10^3$ L mol^{-1} cm^{-1}. Bis(triphenylphosphine)iminium trisulfur trinitride, $PPN^+S_3N_3^-$, was prepared by the reaction of $PPN^+N_3^-$ [14] with S_4N_4 (1:1 mole ratio) in absolute ethanol, using the procedure already described for the preparation of $S_3N_3^-$ salts.[15] The crude yellow product was filtered off under nitrogen, extracted with pentane to remove cyclo-S_8, and recrystallized from anhydrous CH_2Cl_2/methanol to give lime-green blocks (66% yield), which decompose slowly on prolonged exposure to air. $PPN^+S_3N_3^-$ showed infrared bands characteristic of the $S_3N_3^-$ ion at 925 vw and 642 s cm^{-1}.[15] The UV–visible spectrum also exhibited a characteristic band at 365 nm, $\epsilon \sim 3.9 \times 10^3$ L mol^{-1} cm^{-1}.[15]

Piperidine was stored over molecular sieves and distilled before use. Acetonitrile (reagent grade) was dried by distillation from P_2O_5 followed by distillation from calcium hydride. Ethanol and methanol (reagent grade) were dried by distillation from magnesium. All distillations of solvents and all reactions were carried out under an atmosphere of nitrogen (99.99% purity) passed through Ridox and silica gel.

Instrumentation. Routine infrared spectra (CsI windows) were recorded as Nujol mulls on a Perkin-Elmer 467 grating spectrophotometer.

UV–visible spectra were obtained by using a Cary 14 spectrophotometer. The infrared spectra of $PPN^+S_4N^-$ and $PPN^+S_4*N^-$ were obtained for Nujol mulls (CsI) and solutions in CH_3CN (KBr), using a Perkin-Elmer Model 850 ratio-recording spectrophotometer with attached computer for data handling. The Raman spectra were recorded on a Jarrell-Ash Model 25-100 double monochromator calibrated with carbon tetrachloride. A Coherent Radiation CR3 argon-ion laser was used to produce exciting lines at 457.9, 488.0, and 514.5 nm. Samples were mounted in a 6-cm diameter ring which was rotated at about 1000 rpm to prevent thermal decomposition.

Thermolysis of $PPN^+S_4N_5^-$. **A.** A slurry of $PNP^+S_4N_5^-$ (1.008 g, 1.37 mmol) in degassed acetonitrile (30 mL) was heated to reflux, producing a yellow solution which slowly turned orange after a few minutes. Over the next 6 h the solution went through a series of color changes, passing from orange to red to deep red-green, and finally to deep blue. Heating was continued for another 16 h and then the mixture was cooled to 0 °C, whereupon a few crystals (<0.02 g) of cyclo-S_8 appeared, which were filtered off under nitrogen. The filtrate was evaporated in vacuo to approximately 15 mL and then cooled to -10 °C overnight. The following day the solution was filtered to leave lustrous, deep blue crystals of $PPN^+S_4N^-$ (0.467 g, 0.686 mmol, 50%), which were washed with a little cold toluene and sucked dry. Crystals of $PPN^+S_4N^-$ (mp 155–158 °C with decrepitation) have a copper-like metallic sheen and are stable for several hours in air. In solution, the S_4N^- species is very sensitive to traces of oxygen and moisture, decomposing to as yet uncharacterized oxyanions of sulfur. The UV–visible spectrum of $PPN^+S_4N^-$ exhibits a characteristically intense band at 582 nm,[3b] $\epsilon \sim 1.6 \times 10^4$ L mol^{-1} cm^{-1}. The details of the vibrational spectra of the S_4N^- ion are given in the Results and Discussion section.

B. In a second experiment a slurry of $PPN^+S_4N_5^-$ (1.007 g, 1.37 mmol) in degassed acetonitrile (30 mL) was heated to reflux, and the color of the reaction mixture was monitored by visible spectroscopy. As soon as the blue (λ_{max} 582 nm) color of the S_4N^- ion was observed, heating was discontinued and the solution cooled to room temperature. The volume of the solution was reduced to ca. 15 mL in vacuo, and the mixture was cooled to 0 °C for a period of 3 h. The solution was then filtered to reveal a crystalline mixture (0.240 g) containing cyclo-S_8, $PPN^+S_4N_5^-$ (canary-yellow needles), and $PPN^+S_3N_3^-$ (lime-green needles). The latter two components were separated manually and identified by their infrared and UV–visible spectra.

Thermolysis of $PPN^+S_3N_3^-$. A solution of $PPN^+S_3N_3^-$ (0.980 g, 1.47 mmol) in degassed acetonitrile (60 mL) was heated to reflux, whereupon the color of the solution rapidly changed from yellow-green to deep blue. After 7 h at reflux the solution was cooled to room temperature and concentrated in vacuo to ca. 15 mL. The solution was then warmed to redissolve some $PPN^+S_4N^-$ that had crystallized out, and the mixture was then cooled to -10 °C overnight. The solution was filtered and the deep blue crystals of $PPN^+S_4N^-$ were washed with a little cold toluene and sucked dry (0.259 g, 0.380 mmol, 35% based on sulfur). A few flakes of cyclo-S_8 were also present, and these were removed manually from the $PPN^+S_4N^-$.

Preparation of $PPN^+S_4*N^-$. Isotopically enriched $PPN^+S_4*N^-$ (where *N = 30% ^{15}N) was prepared by the thermolysis of $PPN^+S_4*N_5^-$ [16] in acetonitrile, using the procedure described above for $PPN^+S_4N^-$.

X-ray Structural Determination of $PPN^+S_4N^-$. Crystals of $PPN^+S_4N^-$ suitable for X-ray work were obtained from acetonitrile. A crystal with approximate dimensions of 0.2 × 0.2 × 0.3 mm was mounted in a capillary and used for data collection.

Crystal Data (at 23 ± 1 °C): $C_{36}H_{30}N_2P_2S_4$, $M = 680.86$, $F(000) = 708$, triclinic, space group $P\bar{1}$. Based on 25 reflections, the following unit cell parameters were obtained: $a = 11.220$ (2) Å, $b = 16.860$ (3) Å, $c = 8.862$ (2) Å, $\alpha = 99.17$ (1)°, $\beta = 98.04$ (1)°, $\gamma = 71.56°$, V (for $Z = 2$) = 1739.2 Å^3, $d_c = 1.300$ g cm^{-3}, and $\mu = 3.9$ cm^{-1}.

Data Collection and Reduction. Intensity data were collected by using an Enraf-Nonius CAD4 automated diffractometer under the control of a PDP 11/45 computer, using graphite monochromated Mo Kα radiation ($\lambda = 0.71073$ Å) and a θ–2θ scan rate varying from 4 to 40°/min depending on the intensity of the reflection. A counter aperture width of 2.0 mm, a crystal-to-detector distance of 21 cm, and an incident beam collimator distance of 0.7 mm were used. The scan range was 2θ(Mo Kα_1) - 0.6° to 2θ(Mo Kα_2) + 0.6° and the data range was 0° < 2θ(Mo Kα) < 48°. Moving-crystal moving-counter background counts were taken at each end of the scan range. The ratio of the scan time to background counting time was 2.0. Of the 5616 reflections collected, only the 5454 unique reflections were retained as observed and corrected for Lorentz and polarization effects. Three check reflections were measured periodically, but no changes were observed. Intensities and standard deviations were calculated by using the following formulas:

(7) Mendelsohn, M. H.; Jolly, W. L. *J. Inorg. Nucl. Chem.* **1973**, *35*, 95.
(8) (a) Chivers, T.; Drummond, I. *J. Chem. Soc., Chem. Commun.* **1973**, 734. (b) *Inorg. Chem.* **1974**, *13*, 1222.
(9) Pelloux, S.; Roger, J. *C. R. Acad. Sci., Ser. C.* **1970**, *270*, 943.
(10) Zins, M.; Robineau, M.; Brianso-Perucaud, M. C. *C. R. Acad. Sci., Ser. C.* **1975**, *280*, 875.
(11) Villena-Blanco, M.; Jolly, W. L. *Inorg. Synth.* **1967**, *9*, 98.
(12) Bojes, J.; Chivers, T.; Drummond, I.; Maclean, G. *Inorg. Chem.* **1978**, *17*, 3668.
(13) Flues, W.; Scherer, O. J.; Weiss, J.; Wolmershäuser, G. *Angew. Chem., Int. Ed. Engl.* **1976**, *15*, 379.
(14) Ruff, J. K.; Schlientz, W. J. *Inorg. Synth.* **1974**, *15*, 84.
(15) Bojes, J.; Chivers, T. *Inorg. Chem.* **1978**, *17*, 318.

(16) Chivers, T.; Oakley, R. T., unpublished work.

$$I = S(C - RB)$$

$$\sigma(I) = [S^2(C + R^2B) + (pI)^2]^{1/2}$$

where S is the scan rate, C is the total background peak count, R is the ratio of the scan time to background counting time, B is the total background counting time, and p is a factor (here set to 0.05) introduced to downweight intense reflections. Corrections for changes in intensity of the standard reflections, extinction, or absorption were not necessary.

Solution and Refinement of the Structure. The structure was solved by direct methods. Using 434 reflections ($E_{min} = 1.70$) and 2000 phase relationships, a total of 16 phase sets were produced. From an E map prepared from the phase set showing the second best probability statistics (absolute figure of merit $= 1.02$, residual $= 0.31$) a total of 39 atoms was located. These were included in a least-squares refinement, resulting in agreement factors (defined below) of $R = 0.23$ and $R = 0.31$. The remaining nonhydrogen atoms were located in succeeding difference Fourier syntheses. In the refinement procedure the function minimized was $\Sigma w(|F_o| - |F_c|)^2$, where w is defined as $4F_o^2/\sigma^2(F_o^2)$. Scattering factors were taken from ref 17. Anomalous dispersion effects were included in F_c; the values of $\Delta f'$ and $\Delta f''$ are from ref 18. In the final cycles of refinement the 30 phenyl-ring hydrogen atoms were included in calculated positions with C–H $= 0.95$ Å and β_{iso}'s fixed at 7.0 Å². In the full-matrix least-squares refinement (44 atoms, 397 variable parameters), only the 2987 reflections having $F_o^2 > 3\sigma(F_o^2)$ were included, resulting in a final $R = 0.064$ and $R = 0.083$, where

$$R_1 = \Sigma||F_o| - |F_c||/\Sigma|F_o|$$

$$R_2 = [\Sigma w(|F_o| - |F_c|)^2/\Sigma wF_o^2]^{1/2}$$

The esd of an observation of unit weight was 2.26; the maximum parameter shift was 0.07σ. Plots of $\Sigma w(|F_o| - |F_c|)^2$ vs. $|F_o|$, $\lambda^{-1} \sin \theta$, and various classes of indices showed no significant trends.
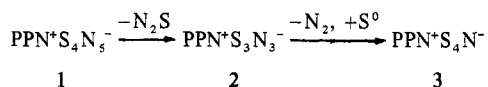
A final difference Fourier map revealed three peaks of 0.4, 0.2, and 0.2 e Å⁻³, which were within ca. 1.2 Å of S(3) and S(4) (hydrogen atoms had appeared on previous maps at 0.3 e Å⁻³). Since the thermal parameters of the sulfurs and N(1) were somewhat large and anisotropic, we ascribe these peaks to anisotropy of the sulfur atoms or a very small amount of disorder.

Theoretical Method. The single determinant closed shell description of S₄N⁻ has been obtained by using the HFS procedure. The frozen core approximation described by Baerends and co-workers[19] was employed for the $1s^2$ core of nitrogen and the $1s^2 2s^2 2p^6$ core of sulfur. The double ζ basis set described by Clementi and Roetti was employed.[20]

Results and Discussion

Synthesis of PPN⁺S₄N⁻. Salts of the S–N anions, S₃N₃⁻ and S₄N₅⁻, with small cations, e.g., alkali metals, exhibit a tendency to explode when subjected to mild pressure or heat.[12,15] Even *n*-Bu₄N⁺S₄N₅⁻ exploded when heated to 100 °C.[21] The dark blue, oily product (λ_{max} 588 nm, in DMF) was not characterized.[21] We have, therefore, prepared salts of these anions with PPN⁺, a cation noted for its ability to stabilize large, strongly nucleophilic metal carbonyl anions.[22] The salts obtained, PPN⁺S₄N₅⁻ (**1**) and PPN⁺S₃N₃⁻ (**2**), are much safer to handle than salts with smaller cations and have allowed us to study the thermolysis of these recently discovered S–N anions.

When a solution of **1** is heated to reflux in acetonitrile for 24 h, a gradual color change from yellow through green to very deep blue is observed. The final product is PPN⁺S₄N⁻ obtained as dark blue crystals with a metallic copper-like lustre. If the thermolysis is stopped immediately after the initial appearance of the blue color (6–7 h), and the solution is cooled to −10 °C, crystals of **2** can be obtained. In a separate experiment it was shown that the transformation **2 → 3** takes place in refluxing acetonitrile.

$$\text{PPN}^+\text{S}_4\text{N}_5^- \xrightarrow{-N_2S} \text{PPN}^+\text{S}_3\text{N}_3^- \xrightarrow{-N_2, +S^0} \text{PPN}^+\text{S}_4\text{N}^-$$

$$\quad\quad \mathbf{1} \quad\quad\quad\quad\quad\quad \mathbf{2} \quad\quad\quad\quad\quad\quad \mathbf{3}$$

This sequence of events is depicted in Figures 1 and 2. The

(17) Cromer, D. T.; Waber, J. T. "International Tables for X-ray Crystallography", Vol. IV; Kynoch Press: Birmingham, England, in press.

(18) Cromer, D. T.; Liberman, D. *J. Chem. Phys.* **1970**, *53*, 1891.

(19) Baerends, E. J.; Ellis, D. E.; Ros, P. *Chem. Phys.* **1973**, *2*, 41.

(20) Clementi, E.; Roetti, C. *At. Data Nucl. Data Tables* **1974**, *14*, 177.

(21) Wolmershäuser, G. Ph.D. Thesis, University of Kaiserslautern, 1976.

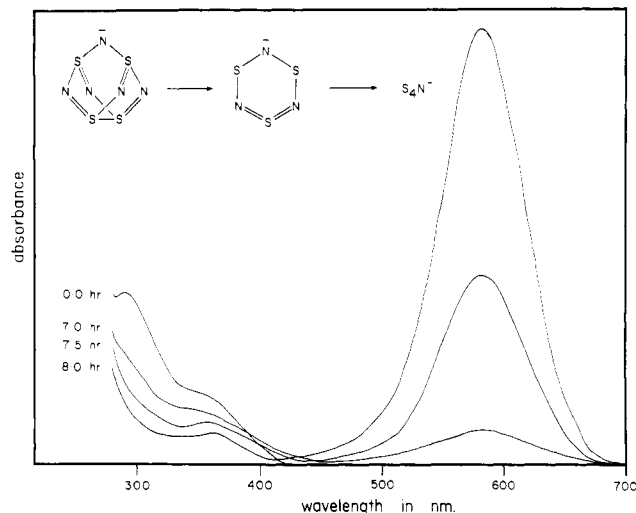(22) For example, see: Ruff, J. K.; White, R. P.; Dahl, L. F. *J. Am. Chem. Soc.* **1971**, *93*, 2159.

Figure 1. UV–visible spectra as a function of time for the transformation S₄N₅⁻ (λ_{max} 293 nm) → S₃N₃⁻ (λ_{max} 365 nm) → S₄N⁻ (λ_{max} 582 nm), starting from a solution of PPN⁺S₄N₅⁻ (ca. 5.0×10^{-2} M) in acetonitrile.
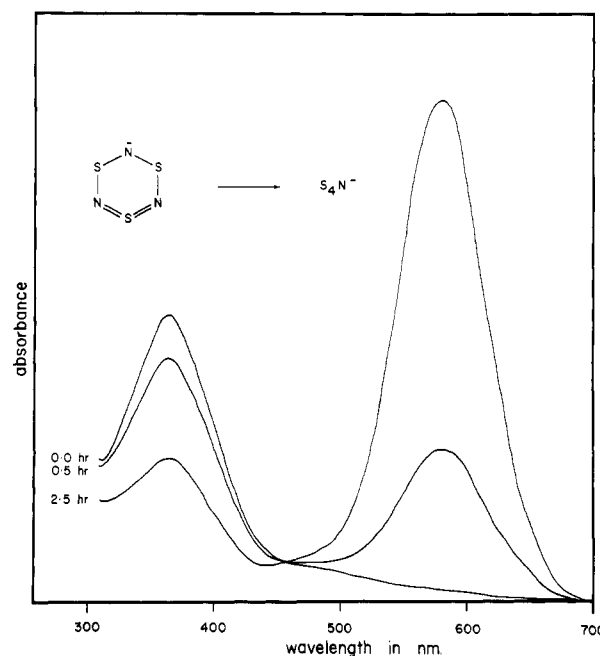

Figure 2. UV–visible spectra as a function of time for the transformation S₃N₃⁻ (λ_{max} 365 nm) → S₄N⁻ (λ_{max} 582 nm), starting from a solution of PPN⁺S₃N₃⁻ (ca. 5.0×10^{-2} M) in acetonitrile.

structures of S₄N₅⁻ [13] and S₃N₃⁻ [23] are known and that of S₄N⁻ is described in this paper. Although we have no direct evidence, the first step appears to involve loss of the neutral molecule N₂S from the S₄N₅⁻ cage to give the six-membered S₃N₃⁻ ring. The existence of N₂S has been postulated,[24a] and ab initio MO calculations favor a linear, unsymmetrical structure,[24b] but no confirmatory experimental evidence for this molecule has been reported. Elemental sulfur is certainly produced in the thermolysis, presumably by disproportionation of N₂S, and it is interesting to note that HFS–SCF calculations for S₄N₅⁻ show that introduction of bridging N⁻ unit into the S₄N₄ framework causes considerable weakening of the S–N framework bonds.[25] Thus, these theoretical results provide a possible rationale for the facile loss of N₂S from S₄N₅⁻. The second step may also involve the initial loss of N₂S

(23) Bojes, J.; Chivers, T.; Laidlaw, W. G.; Trsic, M. *J. Am. Chem. Soc.* **1979**, *101*, 4517.

(24) (a) Powell, F. X. *Chem. Phys. Lett.* **1975**, *33*, 393. (b) Collins, M. P. S.; Duke B. J. *J. Chem. Soc., Dalton Trans.* **1978**, 277.

(25) Chivers, T.; Fielding, L.; Laidlaw, W. G.; Trsic, M. *Inorg. Chem.* **1979**, *18*, 3379.

Table I. Positional and Thermal Parameters and Their Estimated Standard Deviations for PPN⁺S₄N⁻ [a,b]

atom	x	y	z	B_{11}	B_{22}	B_{33}	B_{12}	B_{13}	B_{23}
S(1)	0.4062(2)	0.8482(1)	0.0769(2)	0.0189(3)	0.00707(11)	0.0189(3)	−0.0012(3)	0.0104(5)	−0.0050(3)
S(2)	0.5665(2)	0.7699(1)	0.0254(2)	0.0181(2)	0.00617(9)	0.0177(3)	−0.0041(2)	0.0095(4)	−0.0027(3)
S(3)	0.6749(2)	0.6587(1)	−0.1942(2)	0.0163(2)	0.00920(12)	0.0207(3)	−0.0084(3)	0.0075(5)	−0.0047(3)
S(4)	0.8166(2)	0.6345(2)	−0.0639(3)	0.0169(3)	0.00956(13)	0.0246(4)	−0.0031(3)	0.0064(5)	0.0080(4)
P(1)	0.8771(1)	0.26840(9)	0.3327(2)	0.0076(1)	0.00338(6)	0.0082(2)	−0.0023(1)	0.0032(2)	0.0003(2)
P(2)	0.7267(1)	0.20120(9)	0.4849(2)	0.0068(1)	0.00397(6)	0.0093(2)	−0.0018(1)	0.0036(2)	0.0015(2)
N(1)	0.5542(6)	0.7329(4)	−0.1251(7)	0.0136(6)	0.0085(3)	0.0205(10)	−0.0059(7)	0.0016(14)	−0.0017(10)
N(2)	0.7757(4)	0.2295(3)	0.3655(4)	0.0094(4)	0.0042(2)	0.0083(5)	−0.0042(5)	0.0026(8)	0.0022(5)
C(1)	0.8079(5)	0.3350(3)	0.1998(5)	0.0085(5)	0.0028(2)	0.0080(6)	−0.0016(5)	0.003(1)	−0.0006(6)
C(2)	0.8745(6)	0.3787(4)	0.1500(6)	0.0114(6)	0.0046(3)	0.0108(7)	−0.0042(6)	0.002(1)	0.0026(7)
C(3)	0.8224(7)	0.4264(4)	0.0461(7)	0.0180(8)	0.0049(3)	0.0126(8)	−0.0062(7)	0.005(1)	0.0045(8)
C(4)	0.7016(7)	0.4330(4)	−0.0116(7)	0.0197(9)	0.0047(3)	0.0128(9)	−0.0039(9)	−0.007(2)	0.0058(9)
C(5)	0.6360(7)	0.3901(4)	0.0359(8)	0.0138(8)	0.0066(3)	0.0174(10)	−0.0041(8)	−0.010(2)	0.0090(10)
C(6)	0.6880(6)	0.3411(4)	0.1398(7)	0.0112(6)	0.0050(3)	0.0141(9)	−0.0038(7)	0.001(1)	0.0037(8)
C(7)	1.0139(5)	0.1873(3)	0.2700(6)	0.0084(5)	0.0032(2)	0.0113(7)	−0.0011(6)	0.004(1)	0.0021(7)
C(8)	1.1254(6)	0.2039(4)	0.2669(7)	0.0101(6)	0.0045(3)	0.0194(10)	−0.0015(7)	0.009(1)	0.0036(9)
C(9)	1.2284(6)	0.1424(4)	0.2177(8)	0.0099(6)	0.0060(3)	0.0254(11)	0.0021(8)	0.015(1)	0.0080(10)
C(10)	1.2188(7)	0.0645(4)	0.1698(7)	0.0147(8)	0.0058(3)	0.0201(10)	0.0061(9)	0.017(1)	0.0058(10)
C(11)	1.1081(7)	0.0463(4)	0.1707(7)	0.0178(8)	0.0039(3)	0.0159(9)	−0.0003(8)	0.012(1)	0.0001(9)
C(12)	1.0048(6)	0.1079(4)	0.2203(6)	0.0133(7)	0.0045(3)	0.0100(7)	−0.0032(7)	0.007(1)	−0.003(8)
C(13)	0.9337(5)	0.3304(4)	0.4764(6)	0.0100(5)	0.0048(2)	0.0078(6)	−0.0054(6)	0.003(1)	−0.005(7)
C(14)	1.0264(6)	0.2929(4)	0.5733(7)	0.0119(6)	0.0067(3)	0.0140(9)	−0.0091(7)	−0.001(1)	0.0019(9)
C(15)	1.0595(7)	0.3416(5)	0.6922(8)	0.0173(7)	0.0109(4)	0.0128(10)	−0.0173(8)	−0.006(1)	0.0034(11)
C(16)	1.0001(8)	0.4260(5)	0.7125(8)	0.0275(10)	0.0120(4)	0.0125(10)	−0.0246(9)	0.004(2)	−0.0073(11)
C(17)	0.9109(9)	0.4629(5)	0.6169(8)	0.0279(12)	0.0065(4)	0.0173(11)	−0.0104(10)	0.010(2)	−0.0094(11)
C(18)	0.8754(7)	0.4163(4)	0.4990(7)	0.0175(8)	0.0058(3)	0.0116(9)	−0.0051(9)	0.003(1)	−0.0039(9)
C(19)	0.8440(5)	0.1747(3)	0.6266(5)	0.0087(5)	0.0038(2)	0.0081(6)	−0.0029(5)	0.002(1)	0.0016(7)
C(20)	0.9547(5)	0.1108(3)	0.6010(6)	0.0095(6)	0.0037(2)	0.0106(7)	−0.0017(6)	0.004(1)	0.0000(7)
C(21)	1.0520(6)	0.0915(4)	0.7036(7)	0.0087(6)	0.0056(3)	0.0138(9)	−0.0002(7)	−0.001(1)	0.0035(9)
C(22)	1.0391(7)	0.1369(5)	0.8318(7)	0.0145(8)	0.0076(4)	0.0126(9)	−0.0049(9)	−0.008(1)	0.0045(10)
C(23)	0.9309(8)	0.1983(5)	0.8579(7)	0.0215(11)	0.0089(5)	0.0064(7)	−0.0028(12)	0.000(2)	−0.0033(10)
C(24)	0.8311(6)	0.2172(4)	0.7593(6)	0.0120(7)	0.0055(3)	0.0090(7)	0.0008(8)	0.004(1)	−0.0019(8)
C(25)	0.6824(5)	0.1079(3)	0.4220(6)	0.0074(5)	0.0047(2)	0.0115(7)	−0.0050(5)	0.003(1)	0.009(7)
C(26)	0.6859(6)	0.0502(4)	0.5085(7)	0.0124(6)	0.0063(3)	0.0126(8)	−0.0081(6)	0.0031(1)	0.0025(8)
C(27)	0.6478(6)	−0.0198(4)	0.4590(7)	0.0168(7)	0.0072(3)	0.0167(10)	−0.0129(7)	0.006(1)	0.0029(9)
C(28)	0.6078(6)	−0.0334(4)	0.3229(8)	0.0143(7)	0.0068(3)	0.0226(12)	−0.0131(6)	0.003(2)	−0.0009(11)
C(29)	0.6036(6)	0.0232(4)	0.2350(7)	0.0104(6)	0.0079(4)	0.0150(10)	−0.0077(7)	−0.003(1)	−0.0027(10)
C(30)	0.6414(5)	0.0946(4)	0.2825(7)	0.0090(6)	0.0059(3)	0.0129(8)	−0.0049(6)	−0.001(1)	0.0020(9)
C(31)	0.5919(6)	0.2801(4)	0.5497(7)	0.0094(6)	0.0053(3)	0.0136(8)	0.0007(7)	0.008(1)	0.0048(8)
C(32)	0.4974(7)	0.2611(5)	0.5925(10)	0.0145(7)	0.0075(4)	0.0400(14)	0.0023(9)	0.031(1)	0.0115(12)
C(33)	0.4004(8)	0.3233(7)	0.6520(11)	0.0158(8)	0.0139(6)	0.0498(17)	0.0073(12)	0.039(2)	0.0246(16)
C(34)	0.3950(8)	0.4044(6)	0.6641(9)	0.0201(10)	0.0115(5)	0.0246(13)	0.0177(13)	0.021(2)	0.0136(14)
C(35)	0.4887(10)	0.4250(6)	0.6237(11)	0.0264(13)	0.0067(5)	0.0421(19)	0.0073(13)	0.036(2)	0.0058(16)
C(36)	0.5879(7)	0.3625(5)	0.5663(10)	0.0175(9)	0.0063(4)	0.0383(15)	0.0029(10)	0.033(2)	0.0027(14)

[a] Positional and thermal parameters for the hydrogen atoms can be found in the supplementary material.   [b] The form of the anisotropic thermal parameter is $\exp\{-[B_{11}h^*h^* + B_{22}k^*k^* + B_{33}l^*l^* + B_{12}h^*k^* + B_{13}h^*l^* + B_{23}k^*l^*]\}$.

from $S_3N_3^-$ to produce the hypothetical S_2N^- ion, which would then react with sulfur to give S_4N^-. Such a mechanism cannot be confirmed, since the well-defined isosbestic point in the transformation of $S_3N_3^-$ to S_4N^- (see Figure 2) precludes appreciable concentrations of any intermediate species. However, we have noted that solutions of S_4N^- in CH_2Cl_2 do slowly revert to $S_3N_3^-$ and sulfur (at room temperature). Here again it is difficult to envisage such a process occurring except through an intermediate anion, e.g., S_2N^-. We are currently exploring this problem.

Crystal Structure of PPN⁺S₄N⁻. The positional and thermal parameters for PPN⁺S₄N⁻ are given in Table I. Figure 3 shows ORTEP plots of the cation and anion of PPN⁺S₄N⁻ together with the atomic numbering scheme. Bond lengths and bond angles are summarized in Table II.   The X-ray structure determination reveals that the S_4N^- anion has an unbranched cis,trans chain structure with nitrogen as the central atom, in contrast to the branched-chain structure found for the isoelectronic CS_4^{2-} ion.[10] The S_4N^- chain is essentially planar, the maximum deviation from the least-squares plane through all five atoms being 0.046 Å for N(1) (Table III).   As a result of the orientation of the S(3)–S(4) bond, the S(2)–S(4) distance (3.14 Å) is significantly shorter than the van der Waals separation (3.7 Å) for two sulfur atoms, but the HFS–SCF calculations described below indicate that there is no net bonding interaction between these two atoms. Other intramolecular contacts of interest in the S_4N^- anion are S(2)–S(3)

= 2.773 (2), S(1)–N(1) = 2.856 (5), and S(4)–N(1) = 2.918 (5) Å. The S–S bond lengths in S_4N^- of 1.879 (3) and, to a lesser extent, 1.943 (2) Å are remarkably short compared to the corresponding distances in S_5^{2-}, d(S–S) ~ 2.06 Å,[26] and CS_4^{2-}, d(S–S) = 2.02 Å,[10] and suggest significant multiple-bond character, particularly for the S(3)–S(4) bond. The shortest known S–S bonds, apart from excited states in S_2,[27] are 1.828 Å in $S_2I_4^{2+}$,[28] 1.860 Å in S=SF₂,[29] and 1.882 Å in S_2O.[30]   Short terminal sulfur–sulfur bonds [d(S–S) ~ 1.91 Å] have also been found for the open-chain derivative Ph₃P=NSN=S=S[31] and a related compound containing the –SN=S=S unit.[32]

An unusual feature of the structure of S_4N^- is the marked asymmetry of the central SNS unit, S(3)–N(1) = 1.667 (5) and S(2)–S(1) = 1.521 (5) Å. The shorter S–N bond is adjacent to the longer S–S bond, but the angles at S(2) and S(3) are equal (~110°) within experimental error. The observation of alternating

(26) Kelly, B.; Woodward, P. *J. Chem. Soc., Dalton Trans.* **1976**, 1314.
(27) Steudel, R. *Angew. Chem., Int. Ed. Engl.* **1975**, *14*, 655.
(28) Passmore, J.; Sutherland, G.; Whidden, T.; White, P. S. *J. Chem. Soc., Chem. Commun.* **1980**, 289.
(29) Kuczkowski, R. L. *J. Am. Chem. Soc.* **1964**, *86*, 3617.
(30) Tiemann, E.; Hoeft, J.; Lovas, F. J.; Johnson, D. R. *J. Chem. Phys.* **1974**, *60*, 5000.
(31) Chivers, T.; Oakley, R. T.; Cordes, A. W.; Swepston, P. *J. Chem. Soc., Chem. Commun.* **1980**, 35.
(32) Tamura, C.; Aiba, K.; Sato, S.; Hata, T.; Morimura, S.; Yoshioka, T. *Acta Crystallogr. Sect. B* **1977**, *33*, 3918.

[(Ph₃P)₂N⁺][S₄N⁻] and S₄N⁻$[(Ph_3P)_2N^+][S_4N^-]$ and S_4N^-

J. Am. Chem. Soc., Vol. 102, No. 18, 1980 5777

Table II. Bond Lengths (Å) and Angles (deg) for PPN⁺S₄N⁻

A. Bond Lengths

S(1)–S(2)	1.943(2)	C(4)–C(5)	1.351(7)	C(20)–C(21)	1.375(6)
S(2)–N(1)	1.521(5)	C(5)–C(6)	1.368(6)	C(21)–C(22)	1.371(7)
S(3)–S(4)	1.879(3)	C(7)–C(8)	1.370(6)	C(22)–C(23)	1.348(7)
S(3)–N(1)	1.667(5)	C(7)–C(12)	1.381(6)	C(23)–C(24)	1.367(7)
P(1)–N(2)	1.573(3)	C(8)–C(9)	1.373(6)	C(25)–C(26)	1.381(6)
P(1)–C(1)	1.793(4)	C(9)–C(10)	1.357(8)	C(25)–C(30)	1.394(6)
P(1)–C(7)	1.810(4)	C(10)–C(11)	1.372(8)	C(26)–C(27)	1.375(7)
P(1)–C(13)	1.789(4)	C(11)–C(12)	1.378(6)	C(27)–C(28)	1.362(7)
P(2)–N(2)	1.562(3)	C(13)–C(14)	1.376(6)	C(28)–C(29)	1.374(7)
P(2)–C(19)	1.788(4)	C(13)–C(18)	1.384(6)	C(29)–C(30)	1.392(7)
P(2)–C(25)	1.790(4)	C(14)–C(15)	1.396(7)	C(31)–C(32)	1.337(7)
P(2)–C(31)	1.786(4)	C(15)–C(16)	1.362(9)	C(31)–C(36)	1.359(7)
C(1)–C(2)	1.382(6)	C(16)–C(17)	1.345(9)	C(32)–C(33)	1.374(9)
C(1)–C(6)	1.372(6)	C(17)–C(18)	1.380(7)	C(33)–C(34)	1.336(12)
C(2)–C(3)	1.355(6)	C(19)–C(20)	1.387(5)	C(34)–C(35)	1.333(11)
C(3)–C(4)	1.371(7)	C(19)–C(24)	1.391(5)	C(35)–C(36)	1.383(8)

B. Bond Angles

|					
S(1)–S(2)–N(1)	110.4(2)	C(4)–C(5)–C(6)	121.1(5)	C(20)–C(21)–C(22)	119.2(4)
S(4)–S(3)–N(1)	110.6(2)	C(1)–C(6)–C(5)	120.7(5)	C(21)–C(22)–C(23)	120.3(5)
S(2)–N(1)–S(3)	120.8(3)	P(1)–C(7)–C(8)	121.3(3)	C(22)–C(23)–C(24)	121.9(5)
N(2)–P(1)–C(1)	108.4(2)	P(1)–C(7)–C(12)	119.4(3)	C(19)–C(24)–C(23)	119.0(4)
N(2)–P(1)–C(7)	111.4(2)	C(8)–C(7)–C(12)	119.3(4)	P(2)–C(25)–C(26)	121.6(4)
N(2)–P(1)–C(13)	114.5(2)	C(7)–C(8)–C(9)	121.0(5)	P(2)–C(25)–C(30)	118.6(4)
C(1)–P(1)–C(7)	107.9(2)	C(8)–C(9)–C(10)	119.3(5)	C(26)–C(25)–C(30)	119.8(4)
C(1)–P(1)–C(13)	107.7(2)	C(9)–C(10)–C(11)	121.0(5)	C(25)–C(26)–C(27)	120.7(5)
C(7)–P(1)–C(13)	106.7(2)	C(10)–C(11)–C(12)	119.8(5)	C(26)–C(27)–C(28)	119.9(5)
N(2)–P(2)–C(10)	113.1(2)	C(7)–C(12)–C(11)	119.7(5)	C(27)–C(28)–C(29)	120.3(5)
N(2)–P(2)–C(25)	109.3(2)	P(1)–C(13)–C(14)	121.0(4)	C(28)–C(29)–C(30)	120.9(5)
N(2)–P(2)–C(31)	112.0(2)	P(1)–C(13)–C(18)	119.9(4)	C(25)–C(30)–C(29)	118.4(5)
C(19)–P(2)–C(25)	106.1(2)	C(14)–C(13)–C(18)	118.8(4)	P(2)–C(31)–C(32)	122.4(4)
C(19)–P(2)–C(31)	108.2(2)	C(13)–C(14)–C(15)	119.9(5)	P(2)–C(31)–C(36)	119.6(4)
C(25)–P(2)–C(31)	108.0(2)	C(14)–C(15)–C(16)	120.1(6)	C(32)–C(31)–C(36)	117.8(5)
P(1)–N(2)–P(2)	143.1(2)	C(15)–C(16)–C(17)	120.0(6)	C(31)–C(32)–C(33)	120.6(7)
P(1)–C(1)–C(2)	121.7(3)	C(16)–C(17)–C(18)	121.1(6)	C(32)–C(33)–C(34)	121.3(7)
P(1)–C(1)–C(6)	120.5(3)	C(13)–C(18)–C(17)	120.0(5)	C(33)–C(34)–C(35)	119.2(7)
C(2)–C(1)–C(6)	117.7(4)	P(2)–C(19)–C(20)	118.1(3)	C(34)–C(35)–C(36)	119.7(8)
C(1)–C(2)–C(3)	120.9(4)	P(2)–C(19)–C(24)	123.1(3)	C(31)–C(36)–C(35)	121.4(6)
C(2)–C(3)–C(4)	120.8(5)	C(20)–C(19)–C(24)	118.8(4)		
C(3)–C(4)–C(5)	118.7(5)	C(19)–C(20)–C(21)	120.8(4)		
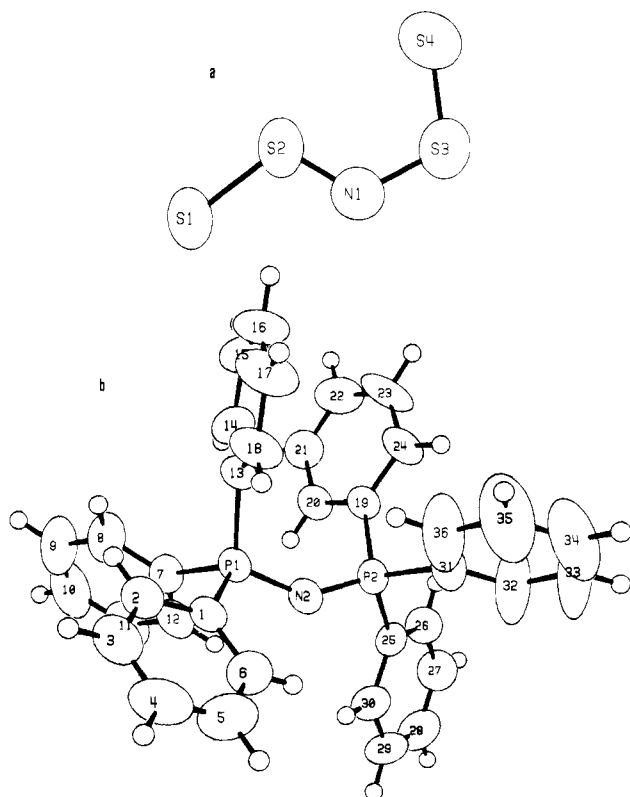
Figure 3. ORTEP plots for (a) the S₄N⁻ anion and (b) the PPN⁺ cation in PPN⁺S₄N⁻.

S–N bond lengths in S–N compounds is not unprecedented, e.g., S₄N₄F₄[33] and S₄N₄²⁺.[34] The origins of this alternation in S₄N⁻ will be discussed later, but it is worth stressing that the energy difference between equal and unequal S–N bonds is likely to be small. For example, one of the forms of the CS₄²⁻ ion found in K₂CS₄·CH₃OH shows two distinct C–S bond lengths of 1.745 and 1.659 Å, while the other form shows essentially equivalent C–S bonds.[10]

The P–N distances of 1.573 (3) and 1.562 (3) Å and the bond angle of 143.1 (2)° at nitrogen in the PPN⁺ cation are not unusual.[35] A pair of stereoscopic drawings of the unit cell of PPN⁺S₄N⁻ are depicted in Figure 4. They clearly show how the bulky PPN⁺ cation protects the relatively small S₄N⁻ anion. A table of intermolecular contacts up to 3.75 Å reveals no significant interactions (see supplementary material).

Vibrational Spectra of the S₄N⁻ Ion. In an earlier publication,[8b] tentative vibrational assignments for the S₄N⁻ ion were made on the basis of a branched-chain structure by analogy with the isoelectronic CS₄²⁻ ion.[9,10] As a result of this X-ray structural determination, it is now clear that those assignments were incorrect. With particular reference to the assignment of vibrational frequencies to the two different S–S bonds in S₄N⁻, we have recorded the infrared and Raman spectra of PPN⁺S₄N⁻ and PPN⁺S₄*N⁻ (where *N = 30% ¹⁵N). The spectra are shown in Figures 5 and 6 and the observed vibrational frequencies and their assignments are summarized in Table IV. On the basis of correlations between S–S stretching frequencies and bond

(33) Wiegers, G. A.; Vos, A. *Acta Crystallogr.* **1963**, *16*, 152.
(34) Gillespie, R. J.; Slim, D. R.; Tyrer, J. D. *J. Chem. Soc., Chem. Commun.* **1977**, 253.
(35) Wilson, R. D.; Bau, R. *J. Am. Chem. Soc.* **1974**, *96*, 7601, and references cited therein.
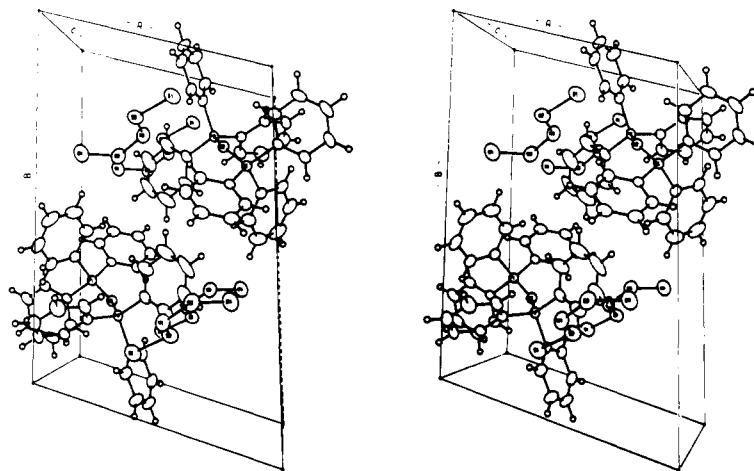
Figure 4. Stereoscopic drawings of unit cell of PPN⁺S₄N⁻.

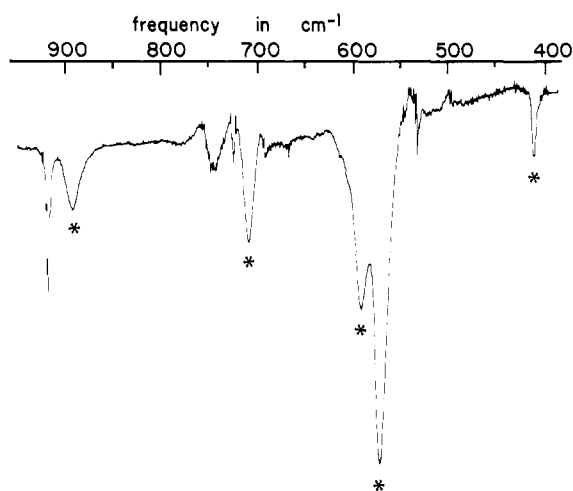**Figure 5.** Difference infrared spectrum of PPN⁺Cl⁻ and PPN⁺S₄N⁻ in acetonitrile solutions. Bands marked with an asterisk are those of the S₄N⁻ anion. Other peaks and inflections are due to imperfect cancellation of solvent and cation bands.
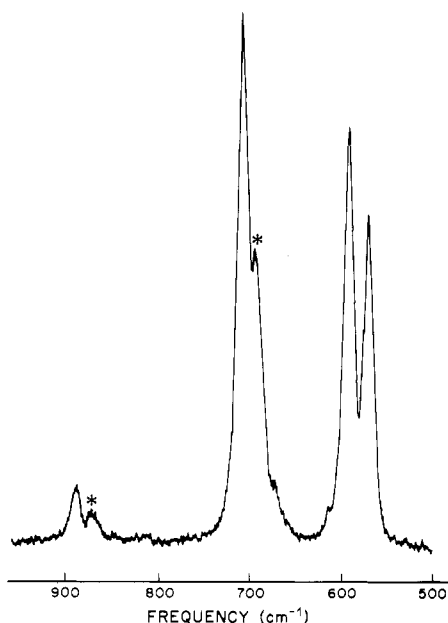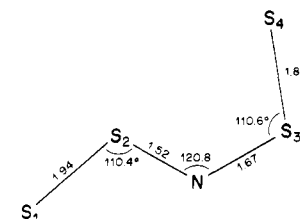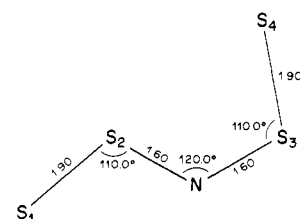

Figure 6. Solid-state (powder) Raman spectrum of PPN⁺S₄*N⁻ obtained with 457.9-nm excitation. Bands marked with an asterisk are not observed in the Raman spectrum of PPN⁺S₄N⁻.

lengths,[27,36] it seems likely that the strong bands observed at ca. 592 and 565 cm⁻¹ in the infrared and Raman spectra of S₄N⁻
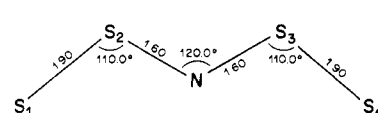

Figure 7. Bond parameters (Å and deg) used in calculations of various conformations of S₄N⁻. The cis and trans designations refer to the geometry of an S–S bond with respect to the remote S–N bond.

correspond to the two S–S stretching vibrations. This assignment is confirmed by the observation that these two bands do not exhibit satellites due to ¹⁵N in the vibrational spectra of PPN⁺S₄*N⁻ (Figure 6). Thus the band at 592 cm⁻¹ is assigned to the stretching mode of the shorter S–S bond (S(3)–S(2)) while the lower frequency band at ca. 565 cm⁻¹ is ascribed to a similar vibration of S(1)–S(2). The relatively high intensity of these bands in the infrared spectrum (Figure 5) is presumably a result of the high polarity of these S–S bonds (vide supra). Two bands are observed above 600 cm⁻¹ in the infrared and Raman spectra of S₄N⁻. The higher frequency band at 892 cm⁻¹ is weak in both the infrared and Raman spectra while the band at 710 cm⁻¹ is of medium intensity in the infrared and very strong in the Raman spectrum (the latter was obscured by solvent and/or cation bands in the spectra of *n*-Bu₄N⁺S₄N⁻ [3b]). The relatively high frequencies of these two bands suggest that they involve stretching of NS bonds and this assignment is confirmed by the observation of ¹⁵N satellites for these bands in both the infrared and Raman spectra

---

(36) Steudel, R. *Z. Naturforsch. B* **1975**, *30*, 281.

Table III. Weighted Least-Squares Planes for S_4N^- [a]

a	b	c	d	atom	x	y	z	distance, Å	esd
0.5815	0.7664	−0.2731	15.3717	atoms in plane					
				S(1)	8.9751	13.4747	0.7454	−0.030(2)	0.002
				S(2)	10.4273	12.2835	0.2463	0.038(2)	0.002
				N(1)	10.2988	11.8714	−1.2123	0.046(7)	0.007
				S(3)	11.3535	10.7677	−1.8825	−0.004(2)	0.002
				S(4)	12.6342	10.2249	−0.6197	−0.020(3)	0.003
0.5954	0.7540	−0.2774	15.4029	atoms in plane					
				S(2)	10.4273	12.2835	0.2463	−0.001(2)	0.002
				N(1)	10.2988	11.8714	−1.2123	0.016(7)	0.007
				S(3)	11.3535	10.7677	−1.8825	−0.002(2)	0.002
				S(4)	12.6342	10.2249	−0.6197	0.001(3)	0.003
				other atoms					
				S(1)	8.9751	13.4747	0.7454	−0.106(2)	0.002
0.6120	0.7453	−0.2644	15.4717	atoms in plane					
				S(2)	10.4273	12.2835	0.2463	0.000(2)	0.002
				N(1)	10.2988	11.8714	−1.2123	0.000(7)	0.007
				S(3)	11.3535	10.7677	−1.8825	0.000(2)	0.002
				other atoms					
				S(1)	8.9751	13.4747	0.7454	−0.133(2)	0.002
				S(4)	12.6342	10.2249	−0.6197	0.045(3)	0.003
0.5530	0.7878	−0.2712	15.3763	atoms in plane					
				S(1)	8.9751	13.4747	0.7454	0.000(2)	0.002
				S(2)	10.4273	12.2835	0.2463	0.000(2)	0.002
				N(1)	10.2988	11.8714	−1.2123	0.000(7)	0.007
				other atoms					
				S(3)	11.3535	10.7677	−1.8825	−0.104(2)	0.002
				S(4)	12.6342	10.2249	−0.6197	−0.166(3)	0.003
0.5996	0.7471	−0.2869	15.3921	atoms in plane					
				N(1)	10.2988	11.8714	−1.2123	0.000(7)	0.007
				S(3)	11.3535	10.7677	−1.8825	0.000(2)	0.002
				S(4)	12.6342	10.2249	−0.6197	0.000(3)	0.003
				other atoms					
				S(1)	8.9751	13.4747	0.7454	−0.158(2)	0.002
				S(2)	10.4273	12.2835	0.2463	−0.034(2)	0.002
0.5796	0.7666	−0.2763	15.3541	atoms in plane					
				S(1)	8.9751	13.4747	0.7454	−0.028(2)	0.002
				S(2)	10.4273	12.2835	0.2463	0.038(2)	0.002
				S(3)	11.3535	10.7677	−1.8825	0.001(2)	0.002
				S(4)	12.6342	10.2249	−0.6197	−0.022(3)	0.003
				other atoms					
				N(1)	10.2988	11.8714	−1.2123	0.051(7)	

[a] Equation of the plane is of the form $ax + by + cz - d = 0$.

Table IV. Vibrational Frequencies (cm⁻¹) and Assignments for the S_4N^- Ion[a]

IR		Raman	
Nujol mull[b]	CH₃CN soln[c]	solid	assignment
*893 w	*892 w	*892 w	ν_{as} (SNS)
*711 m	*709 m	*710 vs	ν_s (SNS)
594 s	592 ms	592 s	ν(S(3)–S(4))
567 vs	562 vs	570 s	ν(S(1)–S(2))
416 w	415 w		d
		227 vw	

[a] Vibrational bands marked with an asterisk showed satellite bands resulting from the presence of ¹⁵N in the spectra of PPN⁺S₄*N⁻. [b] Using CsI windows. [c] In a KBr cell. [d] Tentatively assigned to a bending mode involving the internal sulfurs as the central atoms.

(Figure 7). The observed frequency shifts are 17 (891-cm⁻¹ band) and 14 cm⁻¹ (710-cm⁻¹ band). These shifts compare to 21 and 16 cm⁻¹ calculated for two-center SN vibrations at 891 and 710 cm⁻¹, and 23 cm⁻¹ for a three-center SNS antisymmetric stretch at 891 cm⁻¹. Although the isotopic shifts certainly confirm the involvement of the sulfur-bonded nitrogen in the bands at 710 and 891 cm⁻¹, they do not allow ready distinction between the three-center SNS and two-center SN vibrations. One might reasonably attribute the 892- and 710-cm⁻¹ bands to the stretching modes of the short and long SN bonds, respectively. However, the substantially different intensities of these two bands, despite the rather similar calculated polarities of the SN bonds, make this assignment questionable. The resonance Raman spectra are of some assistance in this connection for it is known that, normally, a three-center symmetric stretching vibration is strongly enhanced. In our case (with exciting lines of 488 and 514.5 nm) we find that the band at 710 cm⁻¹ is increased in intensity, whereas that at 891 cm⁻¹ is not. This suggests that the band at 710 cm⁻¹ represents a vibrational mode with strong characteristics of the symmetric SNS stretch, whereas that at 891 cm⁻¹ has more the characteristics of the antisymmetric stretch. (We might add that the enhanced intensity of the 710-cm⁻¹ band in the resonance Raman spectra also confirms the involvement of the SNS fragment for, as will be argued below, the optical transition is to a molecular orbital, Ψ_{16}, which is strongly associated with the nitrogen and the internal sulfur centers.)

Our assignment of the vibrational bands gains some support from the observation of bands at 906 w, 712 vs, and 583 s cm⁻¹ in the IR spectrum of Ph₃P=NSNSS,[16,31] in which the average S–N bond length is 1.59 Å (cf. 1.59 Å in S₄N⁻). The strong band at 585 cm⁻¹ in the Raman spectrum of Ph₃P=NSNSS can be assigned to the S–S stretching vibration (d(S–S) = 1.908 Å).

Two other bands were observed in the vibrational spectra of S₄N⁻ above 200 cm⁻¹. A weak band at 416 cm⁻¹ only appeared in the infrared spectrum and did not exhibit a ¹⁵N satellite in the spectrum of PPN⁺S₄*N⁻. The Raman band at 227 cm⁻¹ was too weak and broad to detect the presence or absence of a ¹⁵N satellite band. The assignments of these two bands have not been confirmed, but they are likely to be bending modes.

Electronic Structure and Bonding in S_4N^-. Valence bond structures, such as those depicted below, do not give an adequate representation of the electronic distribution in S_4N^-. We have therefore carried out ab initio HFS–SCF calculations for S_4N^-

5780   *J. Am. Chem. Soc., Vol. 102, No. 18, 1980*

Chivers et al.
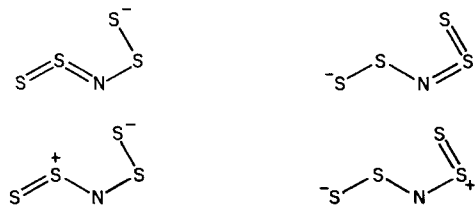
in order to obtain an MO description of the ground-state electronic structure. In an attempt to rationalize the experimentally observed geometry, we have carried out calculations for the following conformations of S_4N^-: (a) experimental cis,trans (CTX), (b) symmetrical cis,trans (CT), and (c) symmetrical trans,trans (TT). These conformations and the bond parameters used in the calculations are shown in Figure 7.

Figure 8 displays the overlap populations and charge densities calculated for the various conformations of S_4N^-. As expected, the nitrogen atom in the experimental conformation, CTX, carries a significant negative charge (-0.35); the terminal sulfurs, however, carry a larger negative charge (-0.42 and -0.44), while the internal sulfurs bear a small positive charge (+0.01 and +0.20). Such charge alternation is typical of open-chain sulfur systems, e.g., sulfanes,[37] and is accentuated in S_4N^- by the central presence of an electronegative nitrogen atom. The relatively high intensity of the S–S stretching bands in the infrared spectra of S_4N^- salts (vide supra and ref 3b and 8b) is undoubtedly a consequence of the polarity of the S–S bonds. The overlap populations found for the S–N linkages (0.53 and 0.55), cf. 0.52 for $S_3N_3^-$,[23] suggest a relatively strong S–N bond. The relative magnitude of the S–S overlap populations is the opposite of that expected on the basis of the observed bond lengths. This inversion of overlap populations is retained in an HFS (X_α) calculation with the much less diffuse single ζ basis and is also observed in the results obtained by using the GAUSSIAN 76 (4-31G basis) HF procedure. In this connection it should also be pointed out that the overlap populations for the CT conformation are 0.77 and 0.64, essentially the same as for the CTX conformation despite the equality of the S–S bond lengths in the former. For the TT conformation the overlap population for both S–S linkages is 0.74. It can be concluded that the inversion of overlap is more a reflection of the cis,trans conformation than of relative bond lengths.

A more detailed analysis of the bonding and charge distribution in S_4N^- can be extracted from the orbital overlap populations given in Table V and from a knowledge of the symmetry of the various orbitals. Thus, we partiton the MOs into three groups: the π orbitals, the σ orbitals, and the nonbonding or lone-pair orbitals. Although desirable, such a classification can only be approximate since a given orbital may have several characteristics; e.g., it may be bonding with reference to one linkage and, yet, antibonding for another.

With the above cautionary statements we begin by noting that the orbitals ψ_7, ψ_{10}, ψ_{12}, ψ_{15}, and the LUMO, ψ_{16}, are π orbitals; i.e., S_4N^- is an 8π-electron system. The lowest of these orbitals, ψ_7 and ψ_{10}, are bonding (π) whereas the HOMO, ψ_{15}, and the LUMO, ψ_{16}, are antibonding (π^*). The intermediate orbital, ψ_{12}, functions as a weak π bond for the S–S linkages and as a lone pair for nitrogen. More precisely, ψ_7 and ψ_{16} are π and π^*, respectively, for the S–N linkages while ψ_{10}, ψ_{12}, and ψ_{15} mainly contribute to the S–S linkages. From the entries in the fourth column of Table V, which gives the orbital overlap population averaged over the two S–N linkages, we note that the net π-type overlap population is $4 \times 0.06 = 0.24$ while from the fifth column we see that the net π-type overlap population averaged over the S–S linkages is $4(0.01 + 0.05 + 0.03 - 0.07) = 0.08$. These overlap populations correspond approximately to a half π bond for each S–N unit and less than a quarter π bond for the S–S units.

(37) Trsic, M.; Laidlaw, W. G. *Int. J. Quantum Chem.* **1980**, *17*, 969.
(38) Wiebanga, E. H.; Havinga, E. E.; Boswijk, K. H. *Adv. Inorg. Chem. Radiochem.* **1961**, *3*, 133.
(39) Migchelson, T.; Vos, A. *Acta Crystallogr.* **1967**, *23*, 796.

Table V. Orbital Overlap Populations for S_4N^-

			averaged orbital overlap populations		orbital overlap populations					self atom orbital overlap populations				
ψ_i	ε_i, au	principal function	$(P_{NS_3} + P_{NS_2})/2$	$(P_{S_1S_2} + P_{S_3S_4})/2$	P_{NS_2}	P_{NS_3}	$P_{S_1S_2}$	$P_{S_3S_4}$	$P_{S_2S_4}$	N	S_1	S_2	S_3	S_4
1	-0.7018	σ_{NS}	0.08	0.01	0.110	0.057	0.008	0.080	0.001	0.36	0.01	0.15	0.08	0.08
2	-0.5643	σ_{SS}	0.03	0.07	0.024	0.026	0.033	0.090	-0.007	0.04	0.05	0.16	0.30	0.11
3	-0.4791	σ_{SS}		0.07	-0.010	0.017	0.086	0.056	0.001	0.15	0.23	0.14	0.07	0.16
4	-0.3890	σ_{NS}	0.04	0.01	0.020	0.060	0.019	-0.004	0.010	0.11	0.23	0.11	0.20	0.21
5	-0.2668	σ^*_{NS}	-0.04	-0.03	-0.052	-0.033	-0.029	-0.021	0.009	0.17	0.29	0.37	0.20	0.23
6	-0.2234	n_S	0.01		-0.024	0.006	-0.004	0.012	0.010	0.16	0.03	0.23	0.26	0.20
7	-0.1891	π_{NS}	0.06	0.01	0.068	0.045	0.014	0.014	0.003	0.26	0.01	0.23	0.15	0.02
8	-0.1875	σ_{NS}	0.03		0.026	0.029	0.002	0.007	0.001	0.18	0.25	0.14	0.12	0.19
9	-0.1207	n_S	-0.01		-0.008	-0.007	-0.003	0.013	-0.010	0.04	0.18	0.23	0.43	0.20
10	-0.1053	π_{SS}		0.05	0.007	-0.007	-0.039	0.070	-0.007		0.08	0.24	0.35	0.16
11	-0.0514	σ^*_{NS}, n_N	-0.06	0.02	-0.056	-0.063	-0.037	-0.001	-0.009	0.44	0.20	0.20	0.16	0.19
12	-0.0349	π_{SS}, n_S		0.03	-0.003	0.010	0.038	0.015	0.001	0.24	0.36	0.04	0.01	0.26
13	-0.0311	n_S		0.01	-0.008	0.011	0.001	0.008	0.027	0.26	0.16	0.08	0.02	0.45
14	-0.0023	n_S		-0.01	-0.007	-0.005	-0.010	-0.005	-0.023	0.06	0.61	0.10	0.05	0.28
15	0.0269	π^*_{SS}		-0.07	-0.002	0.002	-0.054	-0.079	0.015		0.36	0.20	0.32	0.40
16	0.0880	π^*	-0.07	-0.06	-0.076	0.053	-0.061	-0.051	-0.012	0.37	0.20	0.41	0.26	0.19

[(Ph₃P)₂N⁺][S₄N⁻] and S₄N⁻
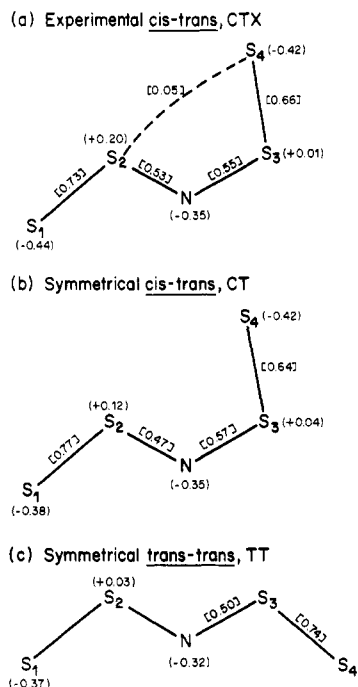
J. Am. Chem. Soc., Vol. 102, No. 18, 1980 5781

Figure 8. Overlap populations in brackets and atomic charges in parentheses for various conformations of S_4N^-.

Let us now consider the σ-bonding framework. From column 4 in Table V we see that the orbitals ψ_1, ψ_2, ψ_4, and ψ_8 make significant σ-bonding contributions to the S–N linkage, whereas ψ_5 and ψ_{11} are antibonding in this region. The net σ_{SN}-type overlap population of $4(0.08 + 0.03 + 0.04 + 0.03 - 0.04 - 0.06) = 0.32$ corresponds to roughly a two-thirds σ bond for each SN region. Referring to the fifth column of Table V, for the SS regions, we see that ψ_2 and ψ_3 make significant σ-bonding contributions while ψ_1, ψ_4, and ψ_{11} make small bonding contributions and this total is reduced by the antibonding contributions of ψ_5. The net σ_{SS}-type overlap population of $4(0.07 + 0.07 + 0.01 + 0.01 + 0.02 - 0.03)$ = 0.60 corresponds to roughly five-quarters of a σ_{SS} bond. Taking the σ and π components of the bonding together, the S–N linkages can be thought of as approximately $(^2/_3\sigma + {}^1/_2\pi)$ bonds, while the S–S linkages are approximately $(^5/_4\sigma + {}^1/_4\pi)$ bonds.

From the last four columns of Table V it is easy to see that ψ_6, ψ_{13}, and ψ_{14} each contribute lone-pair electrons to the terminal sulfurs, whereas ψ_9 plays a similar role for, primarily, the internal sulfurs. In addition ψ_{12} provides some lone-pair character to both the terminal and the internal sulfurs. From the fifth last column of Table V we see that, as well as being antibonding, ψ_{11} also provides lone-pair character to the nitrogen region. The charge buildup around nitrogen and the sulfur centers is, of course, due in part to these lone-pair electrons, but it must be remembered that much of this charge is due to the bonding and antibonding orbitals which are also associated with these centers.

We now turn to the interactions between nonbonded centers, particularly S(2)–S(4), for which the experimental separation is 3.14 Å. These two centers are much closer together in the CT conformations of S_4N^- than they would be in the TT conformation. An analysis of the overlap populations given in Table V reveals that the S(4) lone-pair distributions from ψ_{13} and ψ_{14} do interact significantly with S(2). However, the resulting overlap population, which is bonding (0.027) for ψ_{13}, is essentially canceled by an antibonding (−0.025) contribution from ψ_{14}. It appears, therefore, that the apparent stability of the CTX conformation cannot be rationalized in terms of this "long-bond" interaction. However,

we should point out that the charge distribution obtained for the experimental conformation is more favorable than that which we find for the TT conformation. For example, as Figure 8 shows, the large negative charge (−0.42) of the terminal sulfur S(4) is relatively close to a significant positive charge (+0.20) on the internal sulfur S(2). The larger positive charges on the internal sulfurs in the CTX conformation can also stabilize the very negative nitrogen center. In the case where S(3) and S(4) are trans to the N–S(2) linkage our calculations show that the internal sulfurs carry only very small positive charges (0.03); hence, one would expect less stabilization of the large negative charges on the nitrogen and terminal sulfur centers.

The visible spectrum of the S_4N^- ion exhibits an intense absorption at ca. 580 nm. The transition-state method, suggested by Slater,[40] is commonly used as an approximation to the theoretical value for this transition. In the present case, for a spin-restricted transition state, this procedure yields a value of 680 nm. However, the sum method, shown by Ziegler et al.[41] to be a better approximation, yields a value of 610 nm, which is quite close to the experimental value of 580 nm. The calculation of the transition moments by the $X\nabla$ method, evaluated for the HFS procedure by Trsic et al.,[42] yields a transition moment for the $\psi_{15}\rightarrow\psi_{16}$ (i.e., $\pi^*\rightarrow\pi^*$) transition, which is of order 10^3 greater than that calculated for the $\psi_{14}\rightarrow\psi_{16}$ (i.e., $n\rightarrow\pi^*$) transition. Consequently, it would appear that the strong absorption observed at 580 nm is a HOMO $\pi^*\rightarrow$LUMO π^* transition.

The calculated statistical energies of the three conformations are within 10 kcal mol⁻¹ of one another and one might therefore expect that the details of the conformation of the S_4N^- ion will depend on the nature of the counterion. In particular, it seems possible that a conformation which more closely resembles the symmetrical CT conformation might be found in another salt of S_4N^-. In this connection, we refer to the well-established existence of two forms of trihalide ions, e.g., I_3^-,[38] which is symmetrical in the Ph_4As^+ salt but unsymmetrical in the Cs^+ and NH_4^+ ions. Furthermore, while bulky cations appear to favor the symmetrical form, it is not only cation size which influences the symmetry of the anion. For example, $Et_4N^+I_3^-$ has been shown to contain two structural modifications, one containing symmetrical and the other unsymmetrical I_3^- ions.[39] The synthetic route to S_4N^- salts described in this paper is applicable to salts with other cations and hence should provide an opportunity to test this suggestion.

Note Added in Proof: In a recent X-ray structure determination of $Ph_4As^+S_4N^-$ the S–N bond lengths were found to be S(2)–N(1) = 1.62 and S(3)–N(1) = 1.56 Å (A. W. Cordes and P. Swepston, private communication).

Supplementary Material Available: A listing of structure factor amplitudes, a table of the positional and thermal parameters used for the hydrogen atoms, and a table of intermolecular contacts up to 3.75 Å (27 pages). Ordering information is given on any current masthead page.

(40) Slater, J. C.; Johnson, K. H. *Phys. Rev. B* **1972**, *5*, 844.

(41) Ziegler, T.; Rauk, A.; Baerends, E. J. *Theor. Chim. Acta* **1977**, *46*, 1.

(42) Trsic, M.; Ziegler, T.; Laidlaw, W. G. *Chem. Phys.* **1976**, *15*, 383.